

# UC Santa Barbara

## UC Santa Barbara Previously Published Works

### Title

Molecular-beam epitaxy of p-type m-plane GaN

### Permalink

<https://escholarship.org/uc/item/1rw6k017>

### Journal

Applied Physics Letters, 86(26)

### ISSN

0003-6951

### Authors

McLaurin, M

Mates, T E

Speck, J S

### Publication Date

2005-06-01

Peer reviewed

## Molecular-beam epitaxy of *p*-type *m*-plane GaN

M. McLaurin, T. E. Mates, and J. S. Speck<sup>a)</sup>

Materials Department, University of California, Santa Barbara, California 93106

(Received 7 April 2005; accepted 23 May 2005; published online 22 June 2005)

We report on the plasma-assisted molecular-beam epitaxy of Mg-doped (10 $\bar{1}0$ ) GaN on (10 $\bar{1}0$ ) 6H-SiC. Secondary ion mass spectroscopy measurements show the incorporation of Mg into the GaN films with an enhanced Mg incorporation under N-rich conditions relative to Ga-rich growth. Transport measurements of Mg-doped layers grown under Ga-rich conditions show hole concentrations in the range of  $p=1 \times 10^{18}$  to  $p=7 \times 10^{18}$  cm $^{-3}$  and a dependence between hole concentration and Mg beam equivalent pressure. An anisotropy in in-plane hole mobilities was observed, with the hole mobility parallel to [11 $\bar{2}0$ ] being higher than that parallel to [0001] for the same hole concentration. Mobilities parallel to [11 $\bar{2}0$ ] were as high as  $\sim 11.5$  cm $^2$ /Vs (at  $p \sim 1.8 \times 10^{18}$  cm $^{-3}$ ). © 2005 American Institute of Physics. [DOI: 10.1063/1.1977204]

Internal electric fields produced by discontinuities in the spontaneous and piezoelectric polarization along the [0001] direction of group III wurtzite-nitride heterostructures have been utilized to make devices, such as the dopant-free high electron mobility transistors. However, the polarization-induced electric fields also give rise to the quantum confined Stark effect, which results in the spatial separation of holes and electrons in quantum wells and the subsequent reduction in both the transition probability and the ground-state transition energy.<sup>1,2</sup> In an effort to eliminate the effects of internal polarization-induced electric fields, wurtzite group III nitride films have been grown in the *a*-plane (11 $\bar{2}0$ ) and *m*-plane (10 $\bar{1}0$ ) orientations.<sup>3,4</sup> These growth directions orient the polarization in the plane of heterointerface and, thus, there are no polarization-related electric fields in laterally uniform devices. Plasma-assisted molecular-beam epitaxy (PAMBE)-grown *c*-face GaN suffers from a second deleterious effect in that doping with the commonly used acceptor Mg at high concentrations or low III/V ratios often results in the formation of inversion domains that degrade the quality of the crystal.<sup>5</sup> Since the *c* axis is oriented in the growth plane, inversion should not occur for planar growth of an *m*-plane film. Nonpolar GaN, therefore, is an obvious choice for a route to high-quality relatively highly doped *p* GaN. While both *a*-plane and *m*-plane films have been grown by PAMBE, to date *p*-type doping of nonpolar PAMBE-grown GaN has only been reported for *a*-plane GaN.<sup>6</sup> In this letter, we report on our PAMBE growth of Mg-doped *m*-plane GaN.

Samples were grown in a Varian Gen-II MBE system with Ga and Mg provided by standard elemental effusion cells and active nitrogen produced using a Veeco Unibulb radio-frequency plasma source. Unless otherwise noted, all temperatures reported were measured using a thermocouple located behind the sample. Sample surface temperatures, as measured by optical pyrometry, were typically  $\sim 145$  °C higher than those measured via thermocouple. GaN:Mg layers were grown on pieces of an unintentionally doped (UID) *m*-plane-oriented template grown by MBE on a commercially available 6H *m*-plane SiC substrate at 585 °C. The

UID *m*-plane template consisted of a 40 nm AlN nucleation layer capped with 750 nm GaN grown with an excess of Ga. The template was then removed from the growth system, etched with concentrated HCl to remove Ga droplets, and cleaved into approximately 1 cm wide square pieces. Template pieces were prepared for growth by exposure to acetone, methanol, and isopropanol in an ultrasonic cleaner for 3 min each, bonding with indium to a silicon backing wafer, and heating under a vacuum to 400 °C for 1 h. All samples were grown with 275 W plasma power and a nitrogen flow of 0.3 sccm, which corresponded to a growth rate of approximately 225 nm/h. All sample structures were initiated with the growth of an at least 10 nm thick UID GaN layer grown Ga rich. Transport measurements were performed on GaN:Mg layers that varied in thickness between 500 and 1000 nm, were grown Ga rich, and capped with a 40 nm *p*<sup>+</sup> layer grown at 480 °C.

Carrier type and concentration were determined from Hall effect measurements on lithographically defined Hall bars. The sample sheet resistance and specific contact resistivity were derived from linear transmission line method (TLM) measurements (100  $\times$  200  $\mu$ m $^2$  contacts with 5 to 50  $\mu$ m spacings). Hole mobilities were derived from the measured values of hole concentration and sheet resistance from each *p*-type film. Both the Hall bars and TLM patterns were oriented parallel to both the [0001] and [11 $\bar{2}0$ ] azimuths of the *m*-plane surface and used nonalloyed Pd/Au (20 nm/200 nm) contacts and isolation mesas produced by reactive ion etching. A schematic representation of the Hall bars and TLM structures and their orientation relative to the crystallographic directions of *m*-plane GaN is given in Fig. 1(b). Hall measurements were made using a Lakeshore Cryotronics 7504 Hall effect system. TLM measurements were made using a Sues MicroTec probe station in conjunction with an HP 4145 semiconductor parameter analyzer. No postgrowth treatment was necessary to electrically activate the Mg. Depth dependent profiles of Mg concentration were measured using secondary-ion-mass spectroscopy (SIMS). SIMS analysis was performed in both positive and negative ion modes on a Physical Electronics 6650 DSIMS. For negative ion detection, an 8 kV 300 nA Cs<sup>+</sup> beam was rastered over a 350  $\times$  450  $\mu$ m $^2$  area. For positive ion analysis, a 3 kV O<sub>2</sub><sup>+</sup> beam was rastered over a 300  $\times$  380  $\mu$ m $^2$  area. In both cases,

<sup>a)</sup>Electronic mail: speck@mrl.ucsb.edu

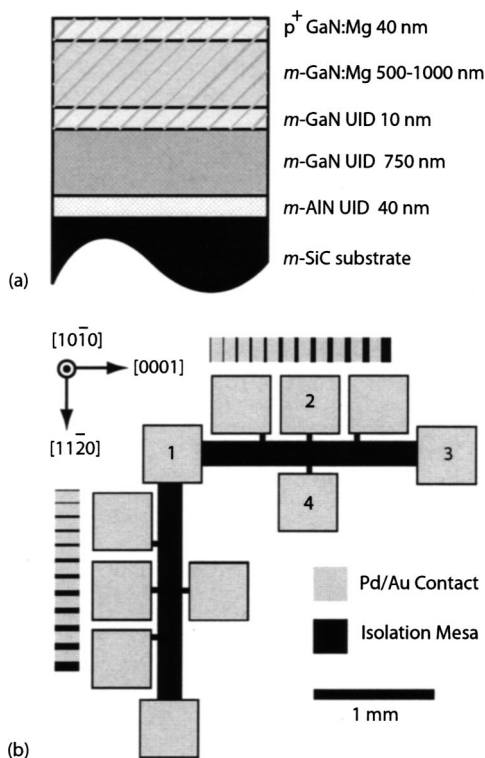


FIG. 1. (a) Schematic representation of transport sample structure. Un-hatched layers belong to the template structure. (b) Schematic representation of Hall bars and TLM patterns used in this study. Hall measurements were taken with the Hall current flowing between Contacts 1 and 3 and Hall voltage measured between Contacts 2 and 4.

secondary ions were accepted only from the central 15% of the sputtered areas. The SIMS system base pressure prior to negative ion analysis was  $9 \times 10^{-11}$  Torr.

Much like *c*-plane and *a*-plane GaN,<sup>7,8</sup> there are two growth regimes of *m*-plane GaN where the growth front contains excess Ga.<sup>9</sup> In the Ga-rich intermediate regime, Ga accumulates as a wetting layer of finite steady-state thickness on the samples' surface, while in the Ga-rich accumulation regime a wetting layer is formed and excess Ga accumulates in the form of droplets. Figure 2 shows the SIMS profile for Mg and Al content in a sample where the III/V flux ratio was varied from N rich to Ga rich and back, while the nominal Mg flux was held constant. The concentration of incorporated Mg was essentially constant between the Ga-rich and intermediate growth, but is higher by almost a factor of 5 under N-rich conditions. This difference in incorporation is not fully explained by the difference in growth rates between the excess-Ga and excess-N growth regimes. In this sample, N-rich growth conditions were achieved by reducing the Ga flux while keeping the nitrogen plasma conditions constant. The N-rich (limited by Ga-flux) growth rate was 160 nm/h, or about 70% that of the Ga-rich and intermediate conditions. Figure 2 is also indicative of the sharp doping profiles that can be achieved with molecular-beam epitaxy (MBE) growth at lower temperatures. The transitions from doped to UID GaN for both Ga-rich and N-rich conditions show relatively steep slopes of  $\sim 7$  nm/decade.

Figure 3 shows representative TLM measurements for samples spanning the range of hole concentrations measured in this work. Since the contact lengths were relatively large (100  $\mu\text{m}$ ) and the Pd/Au contacts were unannealed, it is reasonable to approximate the specific contact resistivity as  $\rho_C$

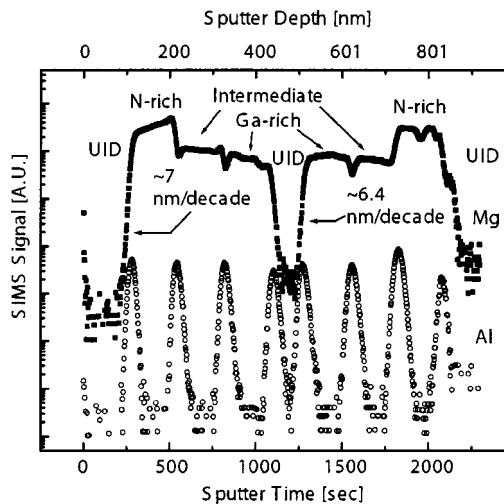


FIG. 2. SIMS data from a sample where the III/V ratio was varied during growth. The Al signal indicates positions of AlGaIn layers marking transitions between different III/V ratios or Mg BEP. UID regions were grown Ga rich. The inverse slope of the Mg signal is indicated for the transitions from intentionally doped to UID material for both Ga-rich growth and N-rich growth.

$=w^2 R_C^2 / R_S$  where  $R_C$  and  $R_S$  are, respectively, the contact and sheet resistances as determined by TLM. Using this method, we measured specific contact resistivities in the range of 1.6 to  $4.7 \times 10^{-4}$  Ohm  $\text{cm}^2$ , which are reasonable values for un-optimized contacts to *p*-type GaN.

We found a clear dependence of room-temperature hole concentration in the transport samples on the nominal beam equivalent pressure (BEP) of Mg [see Fig. 4(a)], and were able to achieve hole concentrations as high as  $7.2 \times 10^{18} \text{ cm}^{-3}$ . This is a significant improvement over typical metalorganic chemical vapor deposition and MBE values for *c*-plane GaN, which typically lie below  $1\text{--}2 \times 10^{18} \text{ cm}^{-3}$ . We speculate that the lower growth temperatures experienced by MBE-grown samples results in a decreased driving force for the formation of compensating defects in the *p*-type GaN. One should expect a similar increase in hole concentration with increasing Mg doping in *c*-plane GaN grown by MBE, however PAMBE-grown *c*-plane GaN is commonly seen to invert in crystallographic orientation (e.g., from Ga face to N face) under heavy Mg doping. We speculate that the observed upper limit of about  $1\text{--}2 \times 10^{18} \text{ cm}^{-3}$  for hole concentrations in PAMBE-grown *c*-face GaN is a result of a com-

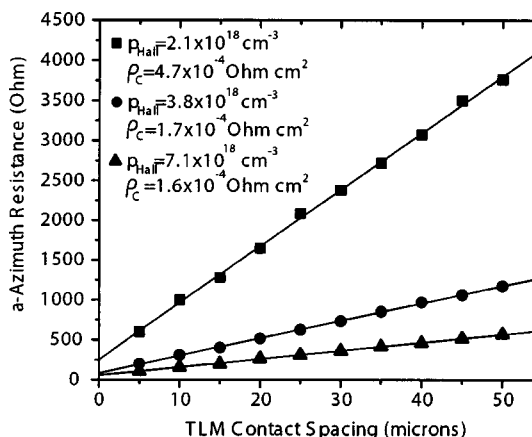


FIG. 3. Representative *a*-azimuth TLM measurements for samples of various hole concentrations. Specific contact resistances are given in the figure.

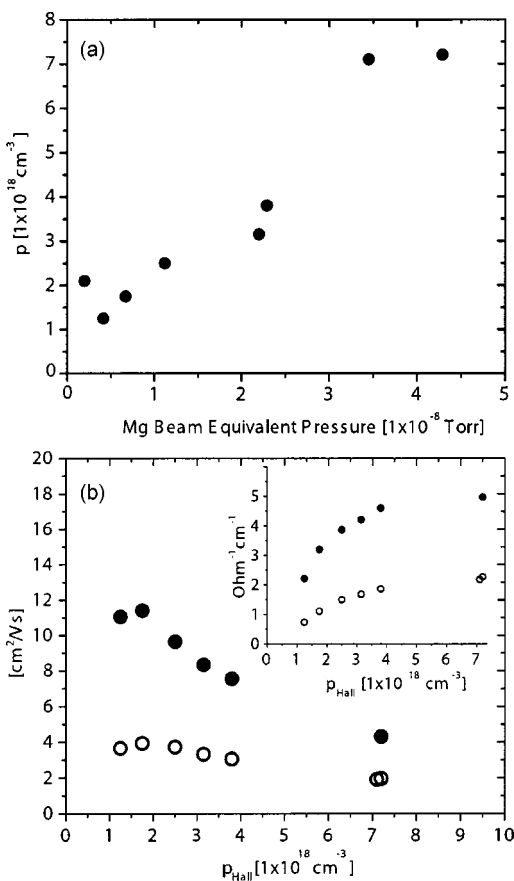


FIG. 4. (a) Hole concentrations as measured by Hall effect versus Mg BEP during growth. (b) Plot of hole mobility in the  $a$  and  $c$  directions (closed and open circles, respectively) vs Hall effect derived carrier concentration. Inset shows plot of sample conductivity derived from hole concentration measured via Hall effect and hole mobilities shown in this figure.

bination of reduced structural quality of the film (i.e., introduction of defects due to the formation of inversion domains that lead to higher scattering rates for holes and hence much lower layer conductivity) and a reduction in the concentration of incorporated Mg in the inversion domains of the crystal.<sup>10</sup> Hall measurements made before and after the removal of the  $p^+$ -contact layer from everywhere but under the metal contacts using a low power reactive ion etch were compared to assess the contribution of the contact layer to the sheet charge of the samples. It was determined that the contact layer's contribution was negligible.

Figure 4(b) shows the measured hole mobilities parallel to the  $[1\bar{1}20]$  and  $[0001]$  as functions of hole concentration. The hole mobility decreased with increasing hole concentration, which is attributed to increased ionized impurity scattering and, as yet, undetermined effects due to the incorporation of Mg at higher doping levels. In-plane hole mobilities were found to be anisotropic, with the mobilities measured parallel to the  $a$  direction two to three times higher than those measured parallel to the  $c$  axis. The anisotropy in hole

mobility has yet to be fully explained, but may be related to anisotropy in the hole effective mass in the plane of the  $m$ -plane GaN surface. Recent theoretical work has shown that light holes should exhibit a similar anisotropy in their effective masses, with the effective mass ratio of  $m_{[0001]}/m_{[1\bar{1}20]}=7.4$  at zero strain, and effective mass ratios ranging from 1 to more than 10 depending on the, as yet, unknown residual strain state of the  $m$ -GaN films.<sup>11</sup> We must also consider nonuniform increases in hole scattering due to the basal plane stacking faults which are ubiquitous in non-polar GaN films.<sup>12,13</sup> The inset of Fig. 4(b) shows the dependence of the conductivity on hole concentration. The sample conductivity increased monotonically with increased hole concentration but appeared to saturate at approximately  $5 \text{ Ohm}^{-1} \text{ cm}^{-1}$  and  $2 \text{ Ohm}^{-1} \text{ cm}^{-1}$  for the  $a$  and  $c$  azimuths, respectively, at the highest hole concentrations.

In summary, we have grown  $p$ -type  $m$ -plane GaN films on 6H  $m$ -plane SiC substrates using Mg as an acceptor. We have measured hole concentrations as high as  $7.2 \times 10^{18} \text{ cm}^{-3}$  without postgrowth annealing and have achieved  $p$ -type conductivity as high as  $5 \text{ Ohm}^{-1} \text{ cm}^{-1}$  parallel to the  $a$  azimuth of the  $m$ -plane GaN films. We measured an anisotropy in hole mobilities, with mobility parallel to the  $[1\bar{1}20]$  azimuth being larger than mobility parallel to the  $[0001]$  at the same hole concentration.

The authors thank Dr. David Look for remeasuring samples and for many useful conversations. This work was supported by the JST/ERATO program at UCSB. This research made use of MRL facilities supported by the National Science Foundation under Award No. DMROO-80034.

- <sup>1</sup>T. Takeuchi, S. Sota, M. Katsuragawa, M. Komori, H. Takeuchi, H. Amano, and I. Akasaki, *Jpn. J. Appl. Phys., Part 2* **36**, L382 (1997).
- <sup>2</sup>V. Fiorentini, F. Bernardini, F. Della Sala, A. DiCarlo, and P. Lugli, *Phys. Rev. B* **60**, 8849 (1999).
- <sup>3</sup>H. M. Ng, *Appl. Phys. Lett.* **80**, 4369 (2002).
- <sup>4</sup>P. Waltereit, O. Brandt, M. Ramsteiner, R. Uecker, P. Reiche, and K. H. Ploog, *J. Cryst. Growth* **218**, 143 (2000).
- <sup>5</sup>V. Ramachandran, R. M. Feenstra, W. L. Sarney, L. Salamanca-Riba, J. E. Northrup, L. T. Romano, and D. W. Greve, *Appl. Phys. Lett.* **75**, 808 (1999).
- <sup>6</sup>R. Armitage, Q. Yang, and E. R. Weber, *MRS Internet J. Nitride Semicond. Res.* **8**, 6 (2003).
- <sup>7</sup>B. Heying, R. Averbeck, L. F. Chen, E. Haus, H. Riechert, and J. S. Speck, *J. Appl. Phys.* **88**, 1855 (2000).
- <sup>8</sup>M. McLaurin, B. Haskell, S. Nakamura, and J. S. Speck, *J. Appl. Phys.* **96**, 327 (2004).
- <sup>9</sup>O. Brandt, Y. J. Sun, L. Daeweritz, and K. H. Ploog, *Phys. Rev. B* **69**, 165326 (2004).
- <sup>10</sup>A. J. Ptak, T. H. Myers, L. T. Romano, C. G. Van de Walle, and J. E. Northrup, *Appl. Phys. Lett.* **78**, 285 (2001).
- <sup>11</sup>H. R. Eisenberg, P. Waltereit, M. McLaurin, H. T. Grahn, S. F. Chichibu, and J. S. Speck (unpublished).
- <sup>12</sup>M. D. Craven, S. H. Lim, F. Wu, J. S. Speck, and S. P. DenBaars, *Appl. Phys. Lett.* **81**, 469 (2002).
- <sup>13</sup>T. Y. Liu, A. Trampert, Y. J. Sun, O. Brandt, and K. H. Ploog, *Philos. Mag. Lett.* **87**, 435 (2004).